

# **The effect of residual water content on preferential adsorption in carbon dioxide – methane – illite clay minerals: A molecular simulation study**

Leebyn Chong<sup>1,2</sup> and Evgeniy M. Myshakin<sup>1,3,\*</sup>

<sup>1</sup>National Energy Technology Laboratory, 626 Cochrans Mill Road, Pittsburgh, PA 15236, USA

<sup>2</sup>Oak Ridge Institute for Science and Education, 100 ORAU Way, Oak Ridge, TN 37830, USA

<sup>3</sup>LRST, 626 Cochran's Mill Road, P.O. Box 10940, Pittsburgh, PA 15236, USA

## **Abstract**

A combination of Monte Carlo and molecular dynamics simulations was carried out to estimate mixed CO<sub>2</sub>/CH<sub>4</sub> adsorption isotherms on illite surfaces in the presence of water. Three bulk phase mixture compositions are explored to study the effect of concentrations on competitive sorption in illite bearing two positions for the isomorphic substitutions. The computed isotherms are compared with those predicted for dry systems to deduce the effect of water on CO<sub>2</sub> and CH<sub>4</sub> interactions with the clay surfaces. The hydration of the counterbalancing ions in pore space is studied to evaluate sorption-desorption processes at the basal clay surfaces. Sensitivity parameters reflecting preferential CO<sub>2</sub>/CH<sub>4</sub> sorption, density profiles, and surface occupancy times are reported and analyzed.

Keywords: molecular simulations; clay minerals; shales; mixed isotherms; carbon dioxide storage and enhanced gas production

## 1 I. Introduction

2 Injection of CO<sub>2</sub> into depleted shale reservoirs is considered a promising method for  
3 permanent CO<sub>2</sub> storage in geological formations that can be accompanied with the benefit of  
4 enhanced natural gas recovery [1, 2]. To improve permeability, a shale reservoir is stimulated  
5 with hydraulic fractures that, together with natural fractures and matrix pores, constitute  
6 potentially available space for CO<sub>2</sub> storage. The presence of hydrocarbons and brine creates  
7 complex interactions between those species, CO<sub>2</sub>, shale pores, and fracture walls. These  
8 interactions control CO<sub>2</sub> storage and gas release, determine transport characteristics of the  
9 mobile fluids, and affect sorption capacity of shale formations [1-4]. Of particular importance is  
10 the capability of CO<sub>2</sub> to preferentially adsorb on organic matter (mostly represented by  
11 kerogen) and on clay mineral surfaces to displace adsorbed methane [1]. Water can compete  
12 with CH<sub>4</sub> and CO<sub>2</sub> for adsorption sites on clays and alter the mineral surface properties. Besides,  
13 water can also affect CO<sub>2</sub> interface density and thickness at supercritical conditions [5].  
14 Characterization of CH<sub>4</sub>, CO<sub>2</sub>, and water interactions with clay minerals is a key factor to reliably  
15 determine carbon storage, enhance gas recovery in shales, and predict reservoir performance.  
16 Shales demonstrate a broad range of brine saturations in pore and fracture space from nearly  
17 dry to condensate-rich shales or tight oil shale formations [6]. Montmorillonite (as a  
18 representative of smectites), kaolinite, and illite compose a substantial portion of the shale  
19 matrix with illite or interstratified illite-smectite as the dominant clay minerals [7-10].

20 At the atomistic level, theoretical studies of adsorption on clay surfaces generally use  
21 grand canonical Monte Carlo (GCMC) simulations carried out at fixed chemical potentials  
22 providing adsorbate concentrations in equilibrium with an external reservoir. Using GCMC  
23 simulations, Kadoura et al. [11] studied the adsorption behavior of CH<sub>4</sub>, CO<sub>2</sub>, and their mixture  
24 at 298.15 K and pressures up to 5 MPa in montmorillonite clays in the presence of water. They  
25 reported adsorption isotherms and selectivity parameters in the presence of 0.4 and 0.2 g/cm<sup>3</sup>  
26 of pre-adsorbed water content in 1.8 and 3.0 nm of basal d<sub>001</sub>-spacing, respectively. The results  
27 have shown that CO<sub>2</sub> uptake and its selectivity over CH<sub>4</sub> increase with the increase of water  
28 content in the interlayer that is attributed to the multilayer adsorption of CO<sub>2</sub> molecules in the  
29 clay. In the presence of water, the CO<sub>2</sub>/CH<sub>4</sub> selectivity increases as the bulk phase pressure

30 increases; the trend opposite to that is found for CO<sub>2</sub>/CH<sub>4</sub> selectivity in dry clay systems [12,  
31 13]. At small interlayer spacings (1.4 vs 2.1 nm), the greater CO<sub>2</sub>/CH<sub>4</sub> selectivity was related to  
32 stronger CO<sub>2</sub> interaction with clay surfaces compared to methane molecules [13]. In other  
33 GCMC studies, the effect of pre-adsorbed water on the adsorption isotherms of pure CO<sub>2</sub> and  
34 CH<sub>4</sub> was estimated for montmorillonite with pore sizes up to 4 nm at 298 K and up to 10 MPa  
35 [14, 15]. Presence of water strongly affects the sorption capacity of clay and diminishes  
36 absorption of both CO<sub>2</sub> and CH<sub>4</sub> forcing those molecules to form the second layer beyond the  
37 water film adsorbed at the surface. The analysis of interactions of pure CO<sub>2</sub> and CH<sub>4</sub> with  
38 montmorillonite surfaces has revealed that the adsorption of CH<sub>4</sub> and CO<sub>2</sub> are dominated by  
39 dispersive force and electrostatic force interactions, respectively. Adsorption of water on clays  
40 is sensitive to the presence of charge and its distribution within clay layers because it increases  
41 electrostatic interactions between water dipoles and clay surfaces [16-20]. Tenney and Cygan  
42 [21] used molecular dynamics (MD) simulations to investigate interfacial behavior and evaluate  
43 contact angles for CO<sub>2</sub>-brine-kaolinite. The siloxane surface of kaolinite is reminiscent of basal  
44 siloxane surfaces of illite and smectites except the absence of charge. The droplet geometry  
45 indicates strong adhesion of the siloxane surface by CO<sub>2</sub> in the presence of brine, while a NaCl  
46 brine droplet in supercritical CO<sub>2</sub> is strongly non-wetting on the same surface. Thus, the  
47 hydrophobic clay surface of neutral kaolinite demonstrates more affinity towards CO<sub>2</sub> than  
48 water molecules. On the other hand, Zhang et al. [22] studied CH<sub>4</sub> adsorption isotherms in  
49 kaolinite with moisture contents ranging from 0 to 5 wt% water by combined Monte Carlo (MC)  
50 and MD simulations at 293.15 K and pressures up to 20 MPa. Adsorption of CH<sub>4</sub> was gradually  
51 suppressed by increasing water content with indications of preferential water adsorption over  
52 methane on both gibbsite and siloxane surfaces.

53 Kumar [23] conducted supercritical CO<sub>2</sub> sorption measurements in dry and water-  
54 imbibed illite clay at 50 °C and pressures up to 12 MPa. The water saturated illite sample  
55 showed a strong suppression of CO<sub>2</sub> sorption compared to the dry sample (from 3.5 to 0.1  
56 mmol/g clay). Busch et al. [10, 24] have performed the CO<sub>2</sub> excess sorption experiments at 45  
57 °C and pressures up to 20 MPa on various clay samples containing mostly Ca-rich  
58 montmorillonite, Na-rich montmorillonite, illite, and kaolinite in the dry and as received

59 moisture state (water contents from 0.1 to 9.7 wt%). For the montmorillonite and illite samples,  
60 higher sorption capacities were observed with the dry samples, whereas wet kaolinite exhibited  
61 higher CO<sub>2</sub> sorption capacities than the dry clay at pressures above 7 MPa (for CO<sub>2</sub>, a transition  
62 to the supercritical state is at T<sub>c</sub> = 31 °C and P<sub>c</sub> = 7.38 MPa). Those experimental data of CO<sub>2</sub>  
63 sorption on the clay mineral surfaces are in general agreement with the MC and MD simulation  
64 data [11, 12, 25-27].

65 Loganathan et al. [28] recently reported CO<sub>2</sub>/CH<sub>4</sub> partitioning in montmorillonite pores  
66 using constant reservoir composition molecular dynamics. They found that CO<sub>2</sub> is preferentially  
67 adsorbed in pore space with the highest CO<sub>2</sub>/CH<sub>4</sub> ratio at a pore thickness of 0.6 nm. That ratio  
68 is decreasing rapidly with an increase of the interlayer distance to the bulk phase CO<sub>2</sub>/CH<sub>4</sub>  
69 compositions. Thus, CO<sub>2</sub> sorption on the clay minerals show a higher CO<sub>2</sub> selectivity and a  
70 stronger interaction energy over methane indicating that CO<sub>2</sub> molecules can competitively  
71 replace CH<sub>4</sub> molecules [11-13]. This suggests that, in shales with clay minerals constituting a  
72 significant portion of rock matrix, CO<sub>2</sub> injection can produce an additional methane volume. The  
73 aqueous phase presence in pore and fracture space may significantly alter sorption/desorption  
74 processes of the fluid mixture at the clay surfaces. Those competitive processes are accounted  
75 through mixed adsorption isotherms [29] that can be used in reservoir simulators for more  
76 realistic predictions of fluid mixture behavior in pore and fracture space of shales. The shale  
77 samples show the broad range of pore size distributions from micro- (<2 nm), meso- (2-50 nm),  
78 to macro-pore (>50 nm) with a majority of pore sizes falling within tens of nm [30]. Previous  
79 simulation works used pore sizes below 4 nm to demonstrate a strong effect of the confining  
80 environment induced by the adjacent clay surfaces on adsorption and/or were focused on  
81 studies of pure CO<sub>2</sub> or CH<sub>4</sub> adsorption within narrow ranges of pressure regimes [11, 13-15, 22,  
82 31-40].

83 The goal of this paper is to investigate preferential adsorption of the binary CO<sub>2</sub>/CH<sub>4</sub>  
84 mixture, pure fluids, and the counter-balancing ions at illite surfaces in the presence of water in  
85 meso-pore space at pressures up to 60 MPa and 355 K, the temperature corresponding to deep  
86 shale formations. In our previous work, the mixed and pure isotherms on dry illitic surfaces  
87 were reported mimicking the conditions in nearly dry shales [12]. Here, the moisture content is

88 introduced in clay pore space to reproduce the residual water saturations existing in tight oil  
89 and condensate-rich shales.

90

## 91 **2. Methodology**

92 Two illite clay structures are constructed using the unit cell formulas,  
93  $KAl_4(OH)_4(Al_{0.5}Si_{3.5}O_{10})_2$  and  $KMgAl_3(OH)_4(Si_4O_{10})_2$ , which are distinguished by the location of  
94 isomorphic substitutions either in the tetrahedral or octahedral layers, respectively. In nature,  
95 the isomorphic substitutions are distributed between octahedral and tetrahedral layers in illite  
96 clays depending of source, rock maturity, and other factors [41]. In this work, the unit cells of  
97 the two limiting idealized illite structures are used to represent responses of clays with  
98 predominant octahedral (O) and tetrahedral (T) substitutions to interaction of fluids in pore  
99 space. Due to the tetrahedral-octahedral-tetrahedral (TOT) arrangement of each illite layer, T  
100 substitutions expose the unbalanced charge at the basal clay surfaces, whereas O substitutions  
101 are located further from the surface resulting in a weakened electrostatic field [42-44]. The illite  
102 structures represent  $4 \times 2 \times 1$  supercells consisting of 328 atoms (8 of which are potassium  
103 charge-balancing counter-ions) with  $a$  and  $b$  lattice distances equal to 2.08 nm and 1.84 nm,  
104 respectively, under periodic boundary conditions. The basal  $d_{001}$ -spacing is set to 9 nm using the  
105 orthogonal supercell for simplicity.  $K^+$  counter-ions were evenly split to be initially located  
106 above the basal surfaces and were able to move in the pore space. More details of the model  
107 preparation can be found in our previous work [12].

108 Five  $CO_2$ - $CH_4$  compositions were explored ( $CO_2:CH_4$  mole fractions): 1:0, 0.8:0.2, 0.5:0.5,  
109 0.2:0.8, and 0:1. For the mixed  $CO_2$ - $CH_4$  systems within the Gibbs ensemble Monte Carlo  
110 (GEMC) simulation framework, 1000 total ( $CO_2+CH_4$ ) molecules were initially segregated into  
111 bulk phase boxes (e.g., 800  $CO_2$  and 200  $CH_4$  molecules for 0.8:0.2) at starting volumes  
112 consistent with each species' bulk densities for the given temperature and pressure. A third box  
113 represents the clay system with pre-seeded water content. In the cases with one pure bulk  
114 phase (0:1 and 1:0), 500 initial molecules were introduced in a simulation box with gas phase.  
115 500 molecules of pure  $CO_2$  and  $CH_4$  were determined to be sufficient to closely reproduce bulk

116 densities in the property database [45]. The description of the MC moves and acceptance  
117 criteria used in the simulations can be found elsewhere [12].

118 For each of the five compositions and two illite clay structures, two concentrations of  
119 pre-adsorbed water were studied that correspond to 10% and 30% of relative humidity (RH) in  
120 bulk phase. Because water is intended to stay in the pore space, it does not participate in swap  
121 moves between boxes and only performs translation and rotation moves within the clay boxes.  
122 The counter-balancing cations also remain in the pore space and are allowed to have  
123 translational moves within the clay boxes. The pre-seeded water concentrations were  
124 determined using the GCMC simulation of water intercalation in clay pore space. Assuming, for  
125 simplicity, that vapor is an ideal gas and using Equation (1) with a chemical potential for water  
126 (-44.5 kJ/mol at 298 K and 1 atm with the TIP4P force field [46]) derived by Tambach et al. [47]  
127 for RH 100%, the concentrations of water in the pore space were estimated to be  
128 approximately 0.1 and 0.3 g/cm<sup>3</sup> for RH 10 and 30%, respectively. The water content is kept  
129 fixed at these concentrations with the assumption that the carbon dioxide and methane do not  
130 strongly impact the relative humidity in pore space.

$$131 \quad RH = 100 * \exp\left(-\frac{\mu_{water}^{sat} - \mu_{water}}{RT}\right) \quad (1)$$

132 where  $\mu_{water}^{sat}$  and  $\mu_{water}$  are chemical potentials at saturated and undersaturated conditions,  
133 respectively. At RH 30%, the density distributions of water indicate that the aqueous phase  
134 occupies about 40% of total pore space which is close to an average value for wet shale  
135 formations [6].

136 The clay structure, carbon dioxide, methane, and water molecules are described with  
137 the ClayFF [48], EPM2-based [49], Tse-Klein-McDonald (TKM) [50], and TIP4P [46] force fields,  
138 respectively. TIP4P, in a combination with ClayFF, provides diffusion coefficients, density  
139 distributions, and structural orientations for water at montmorillonite and kaolinite siloxane  
140 surfaces similar to the SPC model originally used for the ClayFF parametrization [48, 51]. The  
141 TIP4P+EPM2-based force field combination delivers superior performance against the  
142 SPC+EMP2-based one in predictions of transport properties of CO<sub>2</sub> in water [49]. A discussion  
143 regarding the selection of the force fields for CO<sub>2</sub> and CH<sub>4</sub> can be found in our previous paper  
144 [12]. Due to the mixed force fields, undefined Lennard-Jones parameters for unlike pairs are

145 derived through Lorentz-Berthelot combining rules [52]. The cut-off distances for van der Waals  
146 and electrostatic interaction (Ewald summation) are set at 0.92 nm with a switching distance  
147 starting at 0.82 nm.

148 The isotherms were calculated by GEMC simulations for pure CO<sub>2</sub> and CH<sub>4</sub> and their  
149 mixtures at select relative humidity level up to 60 MPa at 355 K. After the densities and  
150 energies have equilibrated, the final structures of the illite system at 1, 10, 30, and 60 MPa are  
151 studied by MD to sample density profiles. For MD simulations, the illite systems with  
152 intercalated species (after equilibration with GEMC) are replicated into 8 x 4 x 2 supercells. The  
153 new dimensions become 4.16 nm x 3.68 nm x 20 nm. A Nose-Hoover thermostat [53] was  
154 applied, and motion integration was calculated with a leap-frog algorithm [54]. Equilibration  
155 was conducted for at least 10 ns with 0.5 fs timesteps and an additional 5 ns used for  
156 production to collect data. The density profiles were composed of densities averaged over the  
157 last nanosecond that were sampled every 5 ps. GEMC simulations were carried out with the  
158 Towhee simulation package [55] and MD simulations were performed using the GROMACS  
159 package [56]. Fig. 1 depicts the MD simulation system consisting of carbon dioxide, methane,  
160 water, counter-ions residing between the clay layers. To ensure consistency between the  
161 theoretical approaches used in the study, select radial distribution functions (RDFs) were  
162 computed using both GEMC and MD methods, and those RDFs were found to give nearly  
163 identical results [12].

164

### 165 3. Results and Discussion

#### 166 3.1. Adsorption Isotherms

167 Total and excess adsorption isotherms were calculated in a similar way applied for the  
168 dry systems [12]. Fig. 2 compares the total adsorption isotherms calculated for the dry clay  
169 systems with those computed using RH 10 and 30%. At both RH levels, the total adsorption  
170 shows higher densities for carbon dioxide than methane for the 0.5:0.5 mixture and pure  
171 species. The total adsorption of CH<sub>4</sub> and CO<sub>2</sub> decreases with increases of RH indicating that the  
172 presence of water molecules in the pore space diminishes the sorption activity of those  
173 molecules. Fig. 3 displays excess adsorption isotherms for pure CO<sub>2</sub> and CH<sub>4</sub> in dry and wet illite

174 systems using two types of the isomorphic substitutions. Since tetrahedral layers are exposed  
175 to pore space, substitutions in those layers are expected to provide stronger interactions with  
176 water dipoles or polarizable molecules like carbon dioxide than substitutions in octahedral  
177 layers. Fig. 3 shows similar adsorption amounts for both types of isomorphic substitutions for  
178 dry and wet systems at both RH levels. The low sensitivity of CO<sub>2</sub> and CH<sub>4</sub> adsorption is  
179 attributed to a screening effect of potassium ions coordinated at the surfaces [12] and  
180 competition for sorption sites with water in the wet systems.

181 Figs. 4 and 5 display the mixed excess adsorption isotherms for CH<sub>4</sub> and CO<sub>2</sub> at three  
182 compositions of the binary CO<sub>2</sub>/CH<sub>4</sub> mixture in a reservoir. At low pressures, the excess  
183 adsorption increases reaching maxima around 10-20 MPa then decreases and even becomes  
184 negative at high pressures suggesting that the densities at bulk phases become higher than  
185 those in the pore space (Figs. 3-5). With an increase of water content, the isotherms  
186 demonstrate the diminished excess adsorption of CH<sub>4</sub> and CO<sub>2</sub> because of the competition with  
187 water molecules at the surfaces. Similar to the excess adsorption isotherm of pure CO<sub>2</sub> and CH<sub>4</sub>,  
188 the mixed adsorption isotherms also show low sensitivity to the isomorphic substitutions (not  
189 shown). Figs. 3 and 4 indicate that methane adsorption is suppressed by the water presence.  
190 Regardless of composition, water effectively dampens maxima for pure CH<sub>4</sub> and mixed excess  
191 adsorption isotherms. At pressures above 10 MPa, the excess adsorption isotherms are  
192 negative in the presence of water suggesting that methane adsorption is unfavorable at the  
193 clay surfaces.

194 Figs. 3 and 5 show the intriguing behavior of the pure and mixed CO<sub>2</sub> excess adsorption  
195 isotherms demonstrating higher adsorption at RH 30% compared to the dry and RH 10%  
196 systems at low pressures. That is an unexpected result given that the isotherms computed at  
197 RH 10% display systematically lower adsorbed amounts than the system with RH 0% over the  
198 entire pressure range. Thus, the introduction of residual water content at RH 10% provides  
199 strong competition with CO<sub>2</sub> (and CH<sub>4</sub>) at the clay surfaces for adsorption sites. The reasons of  
200 such anomalous enhanced CO<sub>2</sub> excess adsorption at low pressures and RH 30% are discussed in  
201 the next section.

202

### 203 3.2. Density Distributions

204 Fig. 6 shows the density distributions of the species in the pore space of illite with T  
205 substitutions for RH 10% and 30% at 10 MPa. The density profiles for the systems with O  
206 substitutions are similar to T ones (Fig. S1 in Supplementary Material). For both RH levels, water  
207 preferentially adsorbs to the clay surfaces and forms films of 1-2 nm thickness. The carbon  
208 dioxide and methane are expelled to the middle of the pore space and the density profiles  
209 demonstrate peaks behind the density peaks corresponding to adsorbed water. For RH 10%,  
210 the density peaks for CO<sub>2</sub> and CH<sub>4</sub> are clearly defined indicating that those molecules still  
211 experience interactions with the basal clay surfaces. The increase of water content leads to the  
212 widening of the water film thicknesses at the basal surfaces that suppresses CO<sub>2</sub> and CH<sub>4</sub>  
213 adsorption and effectively further reduces the pore width available for CO<sub>2</sub> and CH<sub>4</sub>  
214 intercalation. That reduction causes a remarkable shift in amount of intercalated CO<sub>2</sub> that is  
215 quantified by the density profiles in the middle of pore space. Fig. 6 indicates that water films  
216 provide the effect of confining environment inducing the increase of the CO<sub>2</sub> density in the  
217 middle of the pore space from 150 / 300 kg/m<sup>3</sup> to 250 / 500 kg/m<sup>3</sup> for pure and 0.5:0.5 mixture,  
218 respectively, as RH changes from 10% to 30%. That increase in the amount of CO<sub>2</sub> intercalated  
219 in pore space explains why the excess adsorption isotherms displayed in Figs. 3 and 5 are the  
220 highest for RH 30% at pressures below 10 MPa. Since the calculation of excess adsorption  
221 implies subtraction of a bulk density, the increase of CO<sub>2</sub> concentrations in the pore space  
222 would result in an increase in an excess adsorption value. Thus, at low pressures, the higher  
223 excess CO<sub>2</sub> adsorption at RH 30% compared to RH 0% and 10% is attributed to enhanced carbon  
224 dioxide intercalation in the middle of the pore space, rather than to improved adsorption at the  
225 surfaces (Figs 3 and 5).

226 Separate simulations with gradually decreasing pore widths and only pure CO<sub>2</sub> as an  
227 adsorbent have revealed that at a pore width equal to 4 nm, the density profile in the middle of  
228 the pore space increases to ~550 kg/m<sup>3</sup> which is about 1.8 times larger than densities at larger  
229 distances. That value is comparable to the CO<sub>2</sub> density in the middle of pore space at RH 30%  
230 and 10 MPa. In other words, the CO<sub>2</sub> adsorption enhancement (or more precisely, intercalation  
231 enhancement) computed at RH 30% and low pressures is similar to that induced by the

232 confining environment of the adjacent surfaces. Adsorption amount increase upon the  
233 interlayer distance decrease in clay minerals was reported in previous works by other authors  
234 and attributed to the confining effect of the adjacent clay surfaces [28, 57, 58]. However, the  
235 enhancement caused by residual water adsorbed at clay surfaces and effectively reducing the  
236 available pore space for CO<sub>2</sub> intercalation to a critical width is first reported here, to the best of  
237 the authors' knowledge. Noticeably, the described effect of enhanced intercalation in clay pore  
238 space is found for CO<sub>2</sub> only; methane does not demonstrate such a tendency at low pressures.  
239 This could be related to a smaller pore width required to induce the confining effect for CH<sub>4</sub>.  
240 For example, Yang et al. [59] found enhanced methane density in slit-like quartz pores with  
241 widths below 3 nm, the value outside of pore width ranges considered in this work.

242 Above 20 MPa, the excess CO<sub>2</sub> adsorption at RH 30% falls below the values for RH 0%  
243 and 10% (Fig. 3). Figs. S2 and S3 shows density profiles of the species in the pore space of  
244 tetrahedral and octahedral illite systems, respectively, calculated at 30 MPa. The carbon dioxide  
245 density in the middle of the pore space is estimated to be about 850 kg/m<sup>3</sup> for both RH levels,  
246 similar to the density in the dry systems [12]. Consequently, the excess adsorption is reduced as  
247 RH 0% > 10% > 30% due to diminished CO<sub>2</sub> adsorption and pore volume reduction due to the  
248 presence of water (similar adsorption behavior is found for methane adsorption).

249

### 250 3.3. Selectivity Parameters

251 The selectivity parameters quantify the competitive adsorption in the form of  
252  $(x_{\text{CO}_2}/x_{\text{CH}_4})/(y_{\text{CO}_2}/y_{\text{CH}_4})$  where  $x$  and  $y$  are the mole fractions in the adsorbed and bulk phases,  
253 respectively. Fig. 7 shows selectivity parameters estimated for 0.2:0.8; 0.5:0.5; and 0.8:0.2  
254 CO<sub>2</sub>/CH<sub>4</sub> compositions over 60 MPa of a pressure range for dry systems and RH 10%. The  
255 selectivity with moisture content corresponding to RH 30% was excluded from the analysis  
256 since the density profiles show very limited adsorption of CO<sub>2</sub> and CH<sub>4</sub> at the surfaces (Fig. 6).  
257 As a general trend, the selectivity decreases with pressure and reaches plateaux at high  
258 pressures. At all compositions and pressures, the selectivity remains greater than one indicating  
259 preferential adsorption carbon dioxide over methane. For dry systems, the selectivity is higher  
260 at low pressures than the remaining pressure range. At low pressures, preferential carbon

261 dioxide adsorption is more pronounced because of adsorption site availability. With increasing  
262 pressure, the surface sorption capacity is “saturated” leading to reduced CO<sub>2</sub> adsorption  
263 selectivity [12]. At RH 10%, water adsorbed to the clay surfaces occupies active sites that  
264 otherwise would be taken by CO<sub>2</sub>. That causes decreased selectivity compared to the dry  
265 systems especially at low pressures (Fig. 7). There is no apparent trend for the CO<sub>2</sub>/CH<sub>4</sub>  
266 selectivity for the 0.2:0.8 composition at RH 10%. For the 0.5:0.5 composition, the selectivity  
267 increases up to 5 MPa in line with Kadoura et al. [11] who reported increased selectivity for  
268 CO<sub>2</sub>/CH<sub>4</sub> mixture in wet Na-montmorillonite (with a unit charge equal to -0.75e and 1/2 splitting  
269 in T/O substitutions) up to 5 MPa. However, there are large uncertainties in the estimated  
270 selectivity values originated from using the formula that includes four mole fractions bearing  
271 their own standard deviations.

272 Analyzing Fig. 7 it can be deduced that up to 10-15 MPa the water adsorption and  
273 limited capability of CO<sub>2</sub> and CH<sub>4</sub> to displace water molecules at the clay surfaces contribute to  
274 the CO<sub>2</sub>/CH<sub>4</sub> selectivity declining. With further pressure increase the ratios of CO<sub>2</sub>/CH<sub>4</sub>  
275 concentrations in wet pore space becomes converging to the ratios in dry systems and close to  
276 one (in line with the results of Loganathan et al. [28]) indicating that the effect of the  
277 preferential water adsorption on the adsorption selectivity is diminished.

278

### 279 3.4. Angle Distributions

280 The orientation of the carbon dioxide molecules in pore space is a sensitive parameter  
281 reflecting interactions of those molecules with clay surfaces [57]. CO<sub>2</sub> adsorbed in clay pores is  
282 typically oriented parallel to basal surfaces that provides favorable interactions of OCO atoms  
283 with atoms of the hexagonal siloxane rings [60]. In this work, the last 1 ns out of the 5 ns  
284 production period was used to analyze the snapshots every 5 ps. Fig. 8 shows the population  
285 distribution of the angles formed by the line connecting two oxygen atoms of the CO<sub>2</sub> molecule  
286 and the XY plane that fall within 0±20 degrees, *i.e.* the data captures the CO<sub>2</sub> molecules that are  
287 parallel or close-to-parallel to the clay surfaces with O substitutions (the angle distribution is  
288 similar for T substitutions and is not shown). Fig. 8 indicates that in the dry system, CO<sub>2</sub>  
289 preferentially oriented parallel close to the clay surface. At RH 10%, the peaks showing a trend

290 for CO<sub>2</sub> molecules to be parallel are shifted to the middle of pore space and diminished  
291 reflecting weakened CO<sub>2</sub>-clay interaction because of water presence. At RH 30% water, CO<sub>2</sub>  
292 molecules do not show a preferential orientation over the pore width because adsorbed water  
293 films greatly reduce CO<sub>2</sub> interaction with the clay surfaces. The peaks of angle probability  
294 distributions correlate with the density peaks for the corresponding density profiles showing  
295 that CO<sub>2</sub> adsorption is accompanied with the trend for those molecules to stay parallel to the  
296 illite surfaces. Thus, the shift of the CO<sub>2</sub> orientation at the clay surfaces from parallel in the dry  
297 systems to bulk-like in the systems with RH 30% indicates progressively weakened CO<sub>2</sub>  
298 adsorption with increase of water content.

299

### 300 **3.5. Adsorption and Hydration of K<sup>+</sup> at the Clay Surfaces**

301 In our previous work, it was shown that the ions adsorbed at the dry illite surfaces  
302 strongly affect CO<sub>2</sub> and CH<sub>4</sub> adsorption [12]. Placing ions in the middle of pore space leads to  
303 increasing CO<sub>2</sub>/CH<sub>4</sub> excess adsorption. Charged clay layers provide preferential interaction with  
304 polar molecules like water due to strong electrostatic forces acting between molecular dipoles  
305 and clay surfaces. On the other hand, water can fully hydrate adsorbed ions by participating in a  
306 hydration shell. This process effectively removes both ions and water engaged in solvation from  
307 competition with CO<sub>2</sub> and CH<sub>4</sub> for adsorption sites. This section are dedicated to the analysis of  
308 ion and water dynamics in the water films at two relative humidity levels.

309 The density profiles (Fig. 6) indicate that K<sup>+</sup> stays within the pore volume occupied by  
310 water close to the illite surfaces suggesting that the ions can be either adsorbed at the surface  
311 or fully solvated by water. K<sup>+</sup> ions adsorbed at the surface form inner-sphere (IS) complexes  
312 where the ions are located near the centers of the hexagonal rings formed by the silicon atoms  
313 linked together by basal oxygens and coordinated to basal oxygens [61]. Water oxygens  
314 interacting with the ions create a partial hydration shell. K<sup>+</sup> solvation can also promote outer-  
315 sphere (OS) complexes where an ion is completely solvated by water molecules. To probe the  
316 effect of RH on the dynamic transition of the ions from IS to OS complexation (and *vice versa*),  
317 the K<sup>+</sup> residence time was calculated at the surfaces. The adsorption sites for K<sup>+</sup> are defined as  
318 the centers of the hexagonal rings. The positions of K<sup>+</sup> ions were analyzed over the last 1 ns of

319 the MD trajectories for dry and wet clay systems with pure CO<sub>2</sub> at 10 MPa. An ion is counted as  
320 occupying an adsorption site if it is located within 0.37 nm from at least three basal oxygens.  
321 That cutoff distance is taken as the value just beyond the first peaks of the ion-basal oxygens  
322 RDFs which correspond to the ions adsorbed at the surfaces for all clay systems considered. The  
323 number of the K<sup>+</sup> ions spending the same residence time (*ps*) in the adsorbed state was taken  
324 as a ratio to the total number of the K<sup>+</sup> ions (64) in the systems and plotted in Fig. 9 using a 5 *ps*  
325 residence time “bin”. It should be emphasized that an ion can leave the surface and be re-  
326 adsorbed later. To account for this dynamic process, a computed residence time is the sum of  
327 total time intervals a certain ion spends adsorbed over 1 ns of simulation time.

328 Fig. 9 shows residence times for clay with T and O substitutions and different RH levels  
329 in the presence of CO<sub>2</sub>, which predominantly resides in the middle of the pore space (Fig. 6).  
330 Separate analyses using methane reveals a similar residence time pattern indicating CO<sub>2</sub> and  
331 CH<sub>4</sub> do not exert noticeable influence on the ion hydration. Fig. 9 confirms that the potassium  
332 ions in the dry systems remain adsorbed at the surface. The presence of the water films induces  
333 the potassium ions desorption from the surfaces and formation of the OS complexes. The  
334 increase of water content (RH 30% vs 10%) shifts residence times to lower values meaning that  
335 more ions spent their time solvated by water molecules. Using Fig. 9, it is calculated that within  
336 500-1000 *ps* residence time frame for illite with O substitutions, 100% and 52% of the total ions  
337 are adsorbed at the surface with RH 10 and 30%, respectively. For the clay systems with T  
338 substitutions, those numbers are reduced to 69% and 33% meaning more frequent ion  
339 desorption and longer survival times of the OS complexes compared to illite with O  
340 substitutions. In other words, 2/3 of K<sup>+</sup> ions spend more than the half of the select simulation  
341 time (1000 *ps*) as OS complexes at the surface with T substitutions. This correlates well with Lee  
342 et al. [62] who, using resonant anomalous X-ray reflectivity, interpreted the IS K<sup>+</sup> coverage of  
343 cleaved muscovite surfaces exposed to 3x10<sup>-3</sup> molal K<sup>+</sup> aqueous solution, a concentration  
344 sufficient to yield a cation coverage that nearly satisfies the negative charge of the muscovite  
345 surface. The coverage of IS K<sup>+</sup> was estimated ~0.6 atom/unit cell area (60%) meaning that 40%  
346 of ions can be assigned to OS complexes. The muscovite structure is similar to illite with T  
347 substitutions except that the charge in tetrahedral layer is twice more compared to the systems

348 used in this work. Assuming that larger charge per cell area promotes IS complexation, it is  
349 understandable that muscovite demonstrates a pronounced IS motif. This finding also explains  
350 the stronger adsorption of CO<sub>2</sub> in 1:0 (Fig. 3) and 0.8:0.2 (not shown) compositions at the  
351 surfaces with T substitutions at RH 30%. The effect of ion adsorption is more pronounced for  
352 CO<sub>2</sub> adsorption since CO<sub>2</sub> demonstrates stronger affinity to the clay surfaces than CH<sub>4</sub> [12].

353 More frequent K<sup>+</sup> desorption in the T-substituted systems is counter-intuitive since the  
354 charge produced by an isomorphic substitution is located closer to an adsorbed ion in a  
355 tetrahedral layer than in an octahedral one, therefore, providing stronger interaction with an  
356 ion in the former case. Consequently, in Fig. 9, residence times are expected to be longer in the  
357 clay systems with T substitutions than with O ones. For example, the analysis of Na<sup>+</sup> density  
358 profiles in the interlayer space of CO<sub>2</sub>-H<sub>2</sub>O-montmorillonite and CO<sub>2</sub>-H<sub>2</sub>O-beidellite systems  
359 carrying octahedral and tetrahedral charges, respectively, was reported in Ref. [16]. In  
360 montmorillonite, the density profiles show a peak in the middle of the interlayer space suggesting  
361 that Na<sup>+</sup> forms OS complexes; in beidellite, the density peaks are at the surfaces meaning that  
362 Na<sup>+</sup> forms IS complexes [16]. However, in that work, a *d*<sub>001</sub>-spacing was equal to 1.55 nm or  
363 ~0.9 nm of the interlayer space meaning that the confining effect of the two adjacent clay  
364 surfaces favors the IS complexation at T substitutions. In this work the species are adsorbed at  
365 the clay surfaces in pore space with a width of 9.0 nm. There is no confining effect and since the  
366 charge is split between two T layers, while it is localized in an O layer in the other system,  
367 electrostatic interactions are diminished at the clay surface with T substitutions in a meso-pore  
368 compared to interlayer of swelling clays. In this regard, it is interesting how sodium ions would  
369 adsorb at the clay surfaces with O and T substitutions in the pore space used in this work. The  
370 results reported in Supplementary Material show that the surface with T substitutions provide  
371 greater tendency to form IS complexes with Na<sup>+</sup> than that with O ones at both RH levels  
372 opposite to K<sup>+</sup> behavior. That is attributed to stronger Na<sup>+</sup> interaction to the clay surface with T  
373 substitutions than O ones and a steep potential energy curve for an ion motion perpendicular  
374 the surface. On the other hand, K<sup>+</sup> demonstrates a soft potential for interaction with the  
375 surfaces and is more sensitive to greater availability of water molecules at the favorable  
376 orientations promoting desorption of the ions at the surface with T substitutions.

#### 377 4. Conclusions

378 The adsorption of carbon dioxide, methane, and potassium ions on illite surfaces was  
379 explored at the presence of water using a combination of GEMC and MD at 355 K and pressures  
380 from 1 to 60 MPa. Five CO<sub>2</sub>/CH<sub>4</sub> compositions, two isomorphous substitutions in illite clay layers,  
381 and two levels of relative humidity were studied. The mixed adsorption isotherms in the 9 nm  
382 wide pores revealed that the presence of water suppresses adsorption of CO<sub>2</sub> and CH<sub>4</sub>. The  
383 water molecules preferentially adsorbed at the clay surfaces where they form water films and  
384 limit access to carbon dioxide and methane to the adsorption sites. The excess mixed CO<sub>2</sub>/CH<sub>4</sub>  
385 and pure CH<sub>4</sub> adsorption isotherms show near zero values for methane up to 10 MPa. With  
386 further pressure increases, the methane adsorption became negative meaning no adsorption at  
387 the clay surfaces. That is confirmed with analysis of the methane density profiles indicating no  
388 adsorption peaks at the clay surfaces. Since the illite clay mineral is often a major component of  
389 inorganic matter responsible for hydrocarbon sorption, the implication of this finding is that  
390 enhanced gas recovery due to CO<sub>2</sub> injection in liquid-rich shales should be mostly limited to  
391 desorption from organic matter represented by kerogen and gas displacement in pore space.  
392 Moreover, CO<sub>2</sub>/CH<sub>4</sub> adsorption isotherms obtained from experiments on dried crushed shale  
393 samples or calculated for dry systems are valid only for shale formations with no or very low  
394 moisture content and not applicable for wet shales since even 10% of relative humidity strongly  
395 affects the behavior of these species at the clay surfaces.

396 At pressures up to 10 MPa, the excess adsorption for pure CO<sub>2</sub> and mixed isotherms in  
397 clays with RH 30% demonstrates enhancement compared to the dry and RH 10% systems. That  
398 enhancement is attributed to CO<sub>2</sub> density increase in the pore space induced by the water films  
399 adsorbed at the clay surface. This is the consequence of the confining environment effect  
400 where instead of reduced pore widths, the thickness of water films decreases the effective pore  
401 width that promotes enhanced intercalation of CO<sub>2</sub>.

402 The adsorption of the counter-balancing ions at the charged clay surfaces alters their  
403 wettability and affects the mixed CO<sub>2</sub>/CH<sub>4</sub> and pure adsorption isotherms. Illite with T  
404 substitutions provides better hydration and more frequent desorption of K<sup>+</sup> than illite with O  
405 substitutions. The preferential K<sup>+</sup> desorption from the basal clay surfaces with T substitutions is

406 attributed to availability of water at orientations promoting ion hydration. On the other hand,  
407 the strong interaction of Na<sup>+</sup> and the clay surfaces with T substitutions is the main factor  
408 determining more frequent Na<sup>+</sup> desorption from the clays with O substitutions. Regardless of  
409 charge localization in clay layers, in the presence of water, K<sup>+</sup> ions spend more time adsorbed at  
410 the basal surfaces than Na<sup>+</sup> ions in line with a typical behavior of potassium ions as swelling  
411 inhibitors.

412

### 413 **Acknowledgements**

414 This work was performed in support of the US Department of Energy's Fossil Energy  
415 Crosscutting Technology Research Program. The Research was executed through the NETL  
416 Research and Innovation Center's Hydrate Research Field Work Proposal. This research was  
417 supported in part by an appointment to the National Energy Technology Laboratory Research  
418 Participation Program, sponsored by the U.S. Department of Energy and administered by the  
419 Oak Ridge Institute for Science and Education. Research performed by Leidos Research Support  
420 Team (LRST) staff was conducted under the RSS contract 89243318CFE000003. The authors are  
421 thankful to Prof. Ken Jordan (University of Pittsburgh) and Dr. Dustin Crandall (NETL) for fruitful  
422 discussions and comments on this paper.

423

### 424 **Disclaimer**

425 This work was funded by the Department of Energy, National Energy Technology  
426 Laboratory, an agency of the United States Government, through a support contract with  
427 Leidos Research Support Team (LRST). Neither the United States Government nor any agency  
428 thereof, nor any of their employees, nor LRTS, nor any of their employees, makes any warranty,  
429 expressed or implied, or assumes any legal liability or responsibility for the accuracy,  
430 completeness, or usefulness of any information, apparatus, product, or process disclosed, or  
431 represents that its use would not infringe privately owned rights. Reference herein to any  
432 specific commercial product, process, or service by trade name, trademark, manufacturer, or  
433 otherwise, does not necessarily constitute or imply its endorsement, recommendation, or  
434 favoring by the United States Government or any agency thereof. The views and opinions of

435 authors expressed herein do not necessarily state or reflect those of the United States  
436 Government or any agency thereof.

437

438 **References**

439

- 440 [1] J.S. Levine, I. Fukai, D.J. Soeder, G. Bromhal, R.M. Dilmore, G.D. Guthrie, T. Rodosta, S.  
441 Sanguinito, S. Frailey, C. Gorecki, W. Peck, A.L. Goodman, U.S. DOE NETL methodology for  
442 estimating the prospective CO<sub>2</sub> storage resource of shales at the national and regional scale,  
443 *International Journal of Greenhouse Gas Control*, 51 (2016) 81-94.
- 444 [2] M. Godec, G. Koperna, R. Petrusak, A. Oudinot, Potential for enhanced gas recovery and CO<sub>2</sub>  
445 storage in the Marcellus Shale in the Eastern United States, *International Journal of Coal*  
446 *Geology*, 118 (2013) 95-104.
- 447 [3] R. Middleton, H. Viswanathan, R. Currier, R. Gupta, CO<sub>2</sub> as a fracturing fluid: Potential for  
448 commercial-scale shale gas production and CO<sub>2</sub> sequestration, *Energy Procedia*, 63 (2014)  
449 7780-7784.
- 450 [4] A.A. Chialvo, L. Vlcek, D.R. Cole, Acid Gases in CO<sub>2</sub>-rich Subsurface Geologic Environments,  
451 *Reviews in Mineralogy and Geochemistry*, 77 (2013) 361-398.
- 452 [5] H. Zhang, S.J. Singer, Analysis of the Subcritical Carbon Dioxide–Water Interface, *The Journal*  
453 *of Physical Chemistry A*, 115 (2011) 6285-6296.
- 454 [6] D. Jarvie, Shale Resource Systems for Oil and Gas: Part 1—Shale-gas Resource Systems,  
455 *AAPG Mem.*, 97 (2012).
- 456 [7] L. Hong, J. Jain, V. Romanov, C. Lopano, C. Disenhof, A. Goodman, S. Hedges, D. Soeder, S.  
457 Sanguinito, R. Dilmore, An investigation of factors affecting the interaction of CO<sub>2</sub> and CH<sub>4</sub> on  
458 shale in Appalachian Basin, *Journal of Unconventional Oil and Gas Resources*, 14 (2016) 99-112.
- 459 [8] H. Kumar, D. Elsworth, J.P. Mathews, C. Marone, Permeability evolution in sorbing media:  
460 analogies between organic-rich shale and coal, *Geofluids*, 16 (2015) 43-55.
- 461 [9] R. Dilmore, K. Bruner, C. Wyatt, V. Romanov, A. Goodman, S. Hedges, D. McIntyre, D.  
462 Crandall, M. Gill, C. Disenhof, J. Jain, C. Lopano, K. Aminian, M. Zamirian, A. Mashayekhi, S.  
463 Sanguinito, T. Mroz, D. Soeder, Experimental characterization of Marcellus Shale outcrop  
464 samples, and their Interactions with carbon dioxide and methane, U.S. Department of Energy,  
465 National Energy Technology Laboratory, Morgantown, WV, 2015.
- 466 [10] A. Busch, S. Alles, Y. Gensterblum, D. Prinz, D. Dewhurst, M. Raven, H. Stanjek, B. Krooss,  
467 Carbon dioxide storage potential of shales, *International Journal of Greenhouse Gas Control*, 2  
468 (2008) 297-308.
- 469 [11] A. Kadoura, A.K. Narayanan Nair, S. Sun, Adsorption of carbon dioxide, methane, and their  
470 mixture by montmorillonite in the presence of water, *Microporous and Mesoporous Materials*,  
471 225 (2016) 331-341.
- 472 [12] L. Chong, E.M. Myshakin, Molecular simulations of competitive adsorption of carbon  
473 dioxide – methane mixture on illitic clay surfaces, *Fluid Phase Equilibria*, 472 (2018) 185-195.
- 474 [13] N. Yang, S. Liu, X. Yang, Molecular simulation of preferential adsorption of CO<sub>2</sub> over CH<sub>4</sub> in  
475 Na-montmorillonite clay material, *Applied Surface Science*, 356 (2015) 1262-1271.
- 476 [14] Z. Jin, A. Firoozabadi, Methane and carbon dioxide adsorption in clay-like slit pores by  
477 Monte Carlo simulations, *Fluid Phase Equilibria*, 360 (2013) 456-465.

478 [15] Z. Jin, A. Firoozabadi, Effect of water on methane and carbon dioxide sorption in clay  
479 minerals by Monte Carlo simulations, *Fluid Phase Equilibria*, 382 (2014) 10-20.

480 [16] M. Makaremi, K.D. Jordan, G.D. Guthrie, E.M. Myshakin, Multiphase Monte Carlo and  
481 molecular dynamics simulations of water and CO<sub>2</sub> intercalation in montmorillonite and  
482 beidellite, *The Journal of Physical Chemistry C*, 119 (2015) 15112-15124.

483 [17] E.M. Myshakin, M. Makaremi, V.N. Romanov, K.D. Jordan, G.D. Guthrie, Molecular  
484 dynamics simulations of turbostratic dry and hydrated montmorillonite with intercalated  
485 carbon dioxide, *The Journal of Physical Chemistry. A*, 118 (2014) 7454-7468.

486 [18] G. Zhang, W.A. Al-Saidi, E.M. Myshakin, K.D. Jordan, Dispersion-corrected density  
487 functional theory and classical force field calculations of water loading on a pyrophyllite(001)  
488 surface, *The Journal of Physical Chemistry C*, 116 (2012) 17134-17141.

489 [19] S. Kerisit, J.H. Weare, A.R. Felmy, Structure and dynamics of forsterite–scCO<sub>2</sub>/H<sub>2</sub>O  
490 interfaces as a function of water content, *Geochimica et Cosmochimica Acta*, 84 (2012) 137-  
491 151.

492 [20] L.C. Nielsen, I.C. Bourg, G. Sposito, Predicting CO<sub>2</sub>–water interfacial tension under pressure  
493 and temperature conditions of geologic CO<sub>2</sub> storage, *Geochimica et Cosmochimica Acta*, 81  
494 (2012) 28-38.

495 [21] C.M. Tenney, R.T. Cygan, Molecular simulation of carbon dioxide, brine, and clay mineral  
496 interactions and determination of contact angles, *Environmental Science and Technology*, 48  
497 (2014) 2035-2042.

498 [22] B. Zhang, J. Kang, T. Kang, Effect of water on methane adsorption on the kaolinite (0 0 1)  
499 surface based on molecular simulations, *Applied Surface Science*, 439 (2018) 792-800.

500 [23] S. Kumar, Rock-fluid interaction and phase properties of fluids in nano- and subnano-pores  
501 of shales: Sorption-based studies, in: Department of Petroleum Engineering, Colorado School  
502 of Mines, Golden, CO, 2016.

503 [24] A. Busch, S. Alles, B.M. Krooss, H. Stanjek, D. Dewhurst, Effects of physical sorption and  
504 chemical reactions of CO<sub>2</sub> in shaly caprocks, *Energy Procedia*, 1 (2009) 3229-3235.

505 [25] M. Maruthi Sena, M. Krishnan, Role of cations in adsorption of supercritical carbon dioxide  
506 at smectite mineral–water interfaces: Molecular dynamics and adaptive biasing force  
507 simulation studies, *The Journal of Physical Chemistry C*, 123 (2019) 1170-1184.

508 [26] A. Kadoura, A.K. Narayanan Nair, S. Sun, Molecular dynamics simulations of carbon dioxide,  
509 methane, and their mixture in montmorillonite clay hydrates, *The Journal of Physical Chemistry*  
510 *C*, 120 (2016) 12517-12529.

511 [27] M.M. Sena, C.P. Morrow, R.J. Kirkpatrick, M. Krishnan, Supercritical carbon dioxide at  
512 smectite mineral-water interfaces: Molecular dynamics and adaptive biasing force investigation  
513 of CO<sub>2</sub>/H<sub>2</sub>O mixtures nanoconfined in Na-montmorillonite, *Chemistry of Materials*, 27 (2015)  
514 6946-6959.

515 [28] N. Loganathan, G.M. Bowers, B.F. Ngouana Wakou, A.G. Kalinichev, R.J. Kirkpatrick, A.O.  
516 Yazaydin, Understanding methane/carbon dioxide partitioning in clay nano- and meso-pores  
517 with constant reservoir composition molecular dynamics modeling, *Physical Chemistry*  
518 *Chemical Physics*, (2019).

519 [29] M. Sudibandriyo, S.A. Mohammad, R.L. Robinson, K.A.M. Gasem, Ono–Kondo model for  
520 high-pressure mixed-gas adsorption on activated carbons and coals, *Energy and Fuels*, 25  
521 (2011) 3355-3367.

522 [30] X. Luo, S. Wang, Z. Wang, Z. Jing, M. Lv, Z. Zhai, T. Han, Adsorption of methane, carbon  
523 dioxide and their binary mixtures on Jurassic shale from the Qaidam Basin in China,  
524 *International Journal of Coal Geology*, 150-151 (2015) 210-223.

525 [31] G. Chen, J. Zhang, S. Lu, M. Pervukhina, K. Liu, Q. Xue, H. Tian, S. Tian, J. Li, M.B. Clennell,  
526 D.N. Dewhurst, Adsorption behavior of hydrocarbon on illite, *Energy and Fuels*, 30 (2016) 9114-  
527 9121.

528 [32] J. Zhang, M.B. Clennell, K. Liu, M. Pervukhina, G. Chen, D.N. Dewhurst, Methane and  
529 carbon dioxide adsorption on illite, *Energy and Fuels*, 30 (2016) 10643-10652.

530 [33] S.A. Bagherzadeh, P. Englezos, S. Alavi, J.A. Ripmeester, Influence of hydrated silica  
531 surfaces on interfacial water in the presence of clathrate hydrate forming gases, *The Journal of*  
532 *Physical Chemistry C*, 116 (2012) 24907-24915.

533 [34] T. Bui, A. Phan, D.R. Cole, A. Striolo, Transport mechanism of guest methane in water-filled  
534 nanopores, *The Journal of Physical Chemistry C*, 121 (2017) 15675-15686.

535 [35] G. Gadikota, B. Dazas, G. Rother, M.C. Cheshire, I.C. Bourg, Hydrophobic solvation of gases  
536 (CO<sub>2</sub>, CH<sub>4</sub>, H<sub>2</sub>, Noble Gases) in clay interlayer nanopores, *The Journal of Physical Chemistry C*,  
537 121 (2017) 26539-26550.

538 [36] A. Botan, B. Rotenberg, V. Marry, P. Turq, B. Noetinger, Carbon dioxide in montmorillonite  
539 clay hydrates: Thermodynamics, structure, and transport from molecular simulation, *The*  
540 *Journal of Physical Chemistry C*, 114 (2010) 14962-14969.

541 [37] D.R. Cole, A.A. Chialvo, G. Rother, L. Vlcek, P.T. Cummings, Supercritical fluid behavior at  
542 nanoscale interfaces: Implications for CO<sub>2</sub> sequestration in geologic formations, *Philosophical*  
543 *Magazine*, 90 (2010) 2339-2363.

544 [38] Q. Rao, Y. Leng, Molecular understanding of CO<sub>2</sub> and H<sub>2</sub>O in a montmorillonite clay  
545 interlayer under CO<sub>2</sub> geological sequestration conditions, *The Journal of Physical Chemistry C*,  
546 120 (2016) 2642-2654.

547 [39] Q. Rao, Y. Leng, Methane aqueous fluids in montmorillonite clay interlayer under near-  
548 surface geological conditions: A Grand canonical Monte Carlo and molecular dynamics  
549 simulation study, *The Journal of Physical Chemistry B*, 118 (2014) 10956-10965.

550 [40] Q. Rao, Y. Leng, Effect of layer charge on CO<sub>2</sub> and H<sub>2</sub>O intercalations in swelling clays,  
551 *Langmuir*, 32 (2016) 11366-11374.

552 [41] H.E. Gaudette, J.L. Eades, R.E. Grim, The nature of illite, *Clays and Clay Minerals*, 13 (1964)  
553 33-48.

554 [42] A. Delville, Modeling the clay-water interface, *Langmuir*, 7 (1991) 547-555.

555 [43] W.F. Bleam, Atomic theories of phyllosilicates: Quantum chemistry, statistical mechanics,  
556 electrostatic theory, and crystal chemistry, *Reviews of Geophysics*, 31 (1993) 51-73.

557 [44] L.d. Pablo, M.L. Chávez, A.K. Sum, J.J.d. Pablo, Monte Carlo molecular simulation of the  
558 hydration of Na–montmorillonite at reservoir conditions, *The Journal of Chemical Physics*, 120  
559 (2004) 939-946.

560 [45] E.W. Lemmon, I.H. Bell, M.L. Huber, M.O. McLinden, NIST Standard Reference Database 23:  
561 Reference Fluid Thermodynamic and Transport Properties-REFPROP, Version 10.0, National  
562 Institute of Standards and Technology, in, 2018.

563 [46] W.L. Jorgensen, J. Chandrasekhar, J.D. Madura, R.W. Impey, M.L. Klein, Comparison of  
564 simple potential functions for simulating liquid water, *The Journal of Chemical Physics*, 79  
565 (1983) 926-935.

566 [47] T.J. Tambach, P.G. Bolhuis, E.J. Hensen, B. Smit, Hysteresis in clay swelling induced by  
567 hydrogen bonding: accurate prediction of swelling states, *Langmuir*, 22 (2006) 1223-1234.

568 [48] R.T. Cygan, J.-J. Liang, A.G. Kalinichev, Molecular models of hydroxide, oxyhydroxide, and  
569 clay phases and the development of a general force field, *The Journal of Physical Chemistry B*,  
570 108 (2004) 1255-1266.

571 [49] R.T. Cygan, V.N. Romanov, E.M. Myshakin, Molecular simulation of carbon dioxide capture  
572 by montmorillonite using an accurate and flexible force field, *The Journal of Physical Chemistry*  
573 *C*, 116 (2012) 13079-13091.

574 [50] J.S. Tse, M.L. Klein, I.R. McDonald, Computer simulation studies of the structure I clathrate  
575 hydrates of methane, tetrafluoromethane, cyclopropane, and ethylene oxide, *The Journal of*  
576 *Chemical Physics*, 81 (1984) 6146-6153.

577 [51] S. Teich-McGoldrick, D.B. Hart, M.E. Gordon, S.P. Meserole, M.A. Rodriguez, K. Thurmer,  
578 R.T. Cygan, C. Yuan, G.A. Kimmel, B.D. Kay, R.S. Smith, Methane hydrate formation on clay  
579 mineral surfaces, in ; Sandia National Lab. (SNL-NM), Albuquerque, NM (United States); Pacific  
580 Northwest National Laboratory,, Richland, WA, 2015, pp. Medium: ED; Size: 77 p.

581 [52] M.P. Allen, D.J. Tildesley, *Computer simulation of liquids*, Clarendon Press, 1989.

582 [53] S. Nosé, A unified formulation of the constant temperature molecular dynamics methods,  
583 *The Journal of Chemical Physics*, 81 (1984) 511-519.

584 [54] H.J.C. Berendsen, D. van der Spoel, R. van Drunen, GROMACS: A message-passing parallel  
585 molecular dynamics implementation, *Computer Physics Communications*, 91 (1995) 43-56.

586 [55] M.G. Martin, MCCCSTowhee: a tool for Monte Carlo molecular simulation, *Molecular*  
587 *Simulation*, 39 (2013) 1212-1222.

588 [56] M.J. Abraham, T. Murtola, R. Schulz, S. Páll, J.C. Smith, B. Hess, E. Lindahl, GROMACS: High  
589 performance molecular simulations through multi-level parallelism from laptops to  
590 supercomputers, *SoftwareX*, 1-2 (2015) 19-25.

591 [57] X. Yang, C. Zhang, Structure and diffusion behavior of dense carbon dioxide fluid in clay-like  
592 slit pores by molecular dynamics simulation, *Chemical Physics Letters* 407, (2005).

593 [58] S. Gu, B. Gao, L. Teng, Y. Li, C. Fan, S. Iglauer, D. Zhang, X. Ye, Monte Carlo simulation of  
594 supercritical carbon dioxide adsorption in carbon slit pores, *Energy and Fuels*, 31 (2017) 9717-  
595 9724.

596 [59] L. Yang, X. Zhou, K. Zhang, F. Zeng, Z. Wang, Investigation of dynamical properties of  
597 methane in slit-like quartz pores using molecular simulation, *RSC Advances*, 8 (2018) 33798-  
598 33816.

599 [60] E.M. Myshakin, W.A. Saidi, V.N. Romanov, R.T. Cygan, K.D. Jordan, Molecular dynamics  
600 simulations of carbon dioxide intercalation in hydrated Na-montmorillonite, *The Journal of*  
601 *Physical Chemistry C*, 117 (2013) 11028-11039.

602 [61] D. van der Spoel, P.J. van Maaren, P. Larsson, N. Tîmneanu, Thermodynamics of hydrogen  
603 bonding in Hhydrophilic and hydrophobic media, *The Journal of Physical Chemistry B*, 110  
604 (2006) 4393-4398.

605 [62] S.S. Lee, P. Fenter, K.L. Nagy, N.C. Sturchio, Monovalent ion adsorption at the muscovite  
606 (001)-solution interface: Relationships among ion coverage and speciation, *Interfacial Water*  
607 *Structure, and Substrate Relaxation*, *Langmuir*, 28 (2012) 8637-8650.

608

609

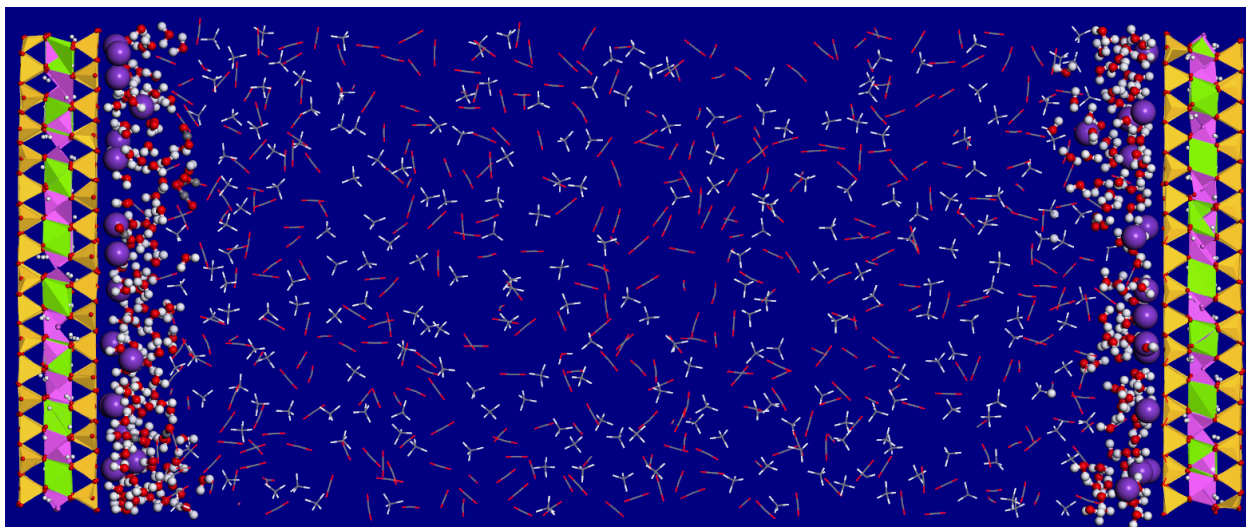


**Fig. 1.** Schematic representation of the equilibrated clay/H<sub>2</sub>O/ CO<sub>2</sub>/CH<sub>4</sub> system at RH 10% and 10 MPa. The color coding of atoms is purple, red, white, gray, yellow, pink, and green for K<sup>+</sup>, O, H, C, Si, Al, and Mg, respectively. For clarity, the water molecules are shown as “balls and sticks” whereas the carbon dioxide and methane are represented as colored lines.

610

611

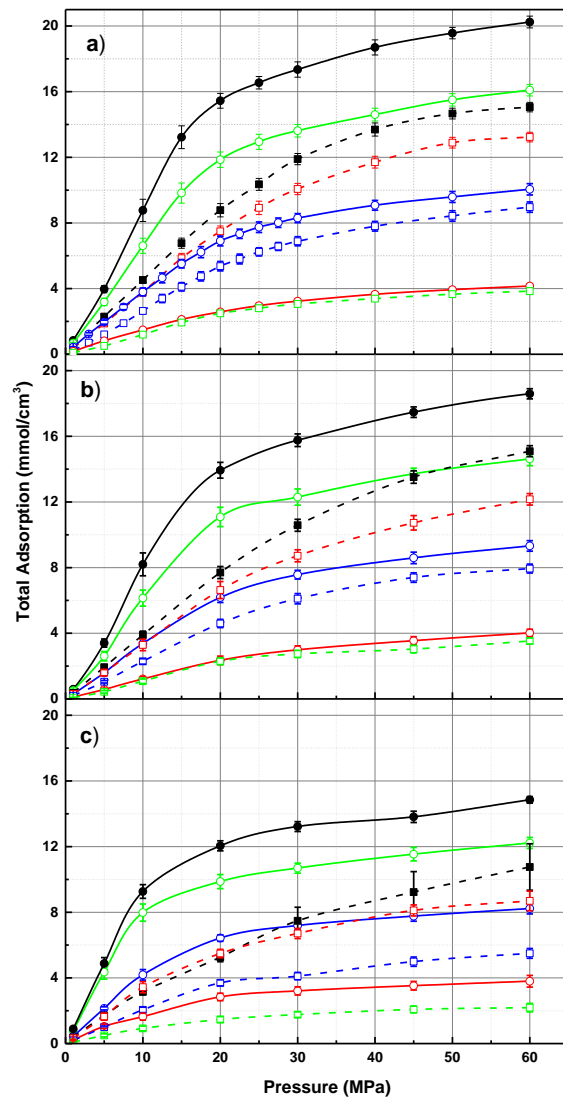


**Fig. 2.** Total adsorption isotherms for ternary  $\text{H}_2\text{O}/\text{CO}_2/\text{CH}_4$  mixtures on illite with tetrahedral substitutions using RH equal to **a)** 0%, **b)** 10%, and **c)** 30% at 355 K. The black, green, blue, and red lines are for 1:0/0:1, 0.8:0.2, 0.5:0.5, and 0.2:0.8 molar fractions, respectively. The solid and dashed lines are for  $\text{CO}_2$  and  $\text{CH}_4$ , respectively.

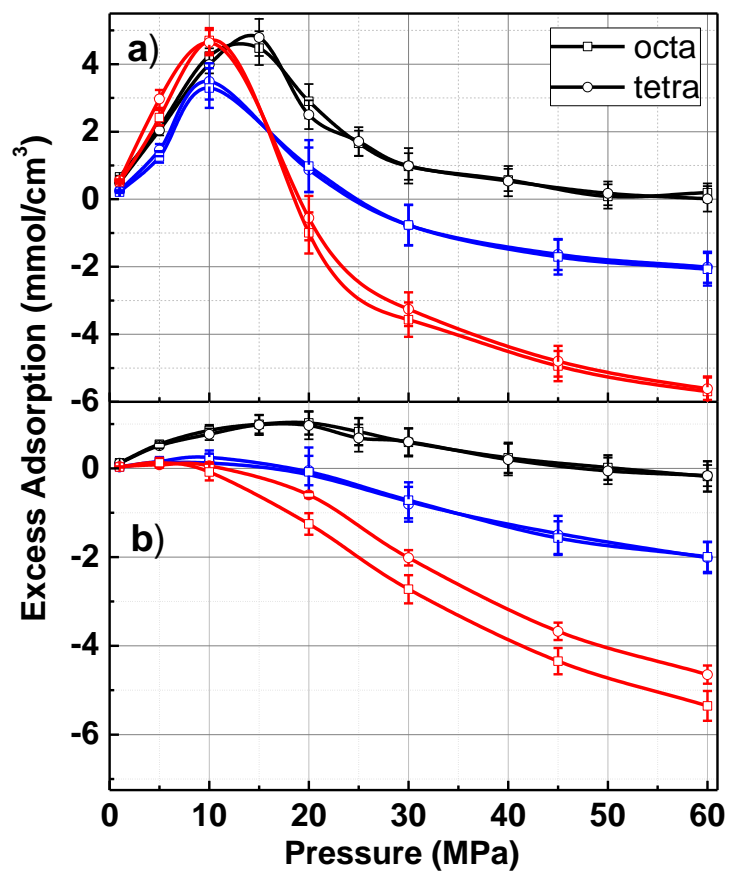
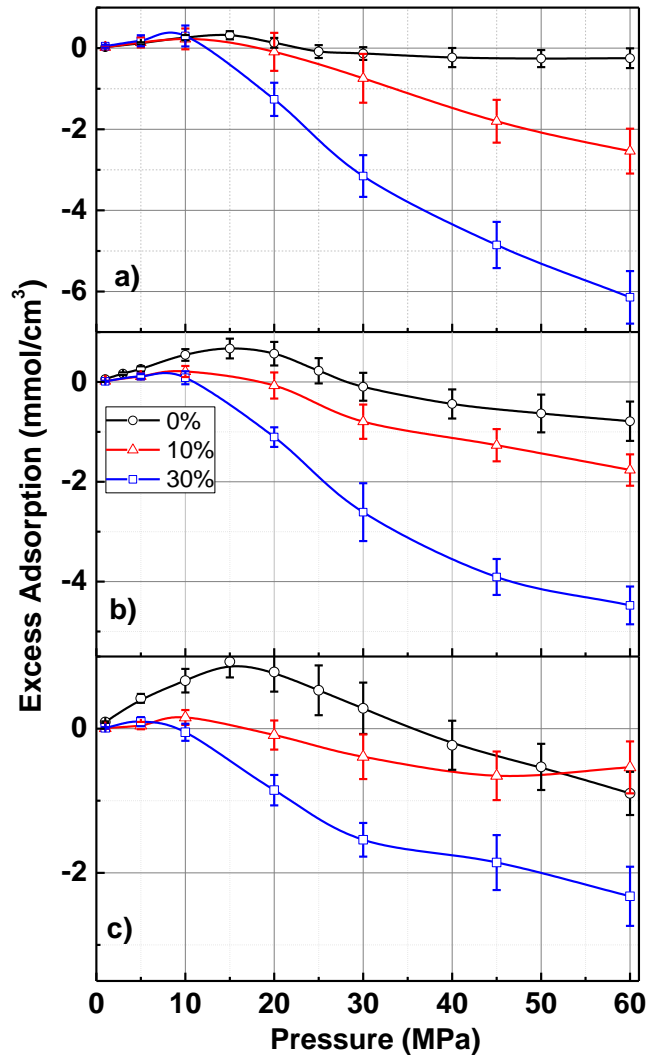
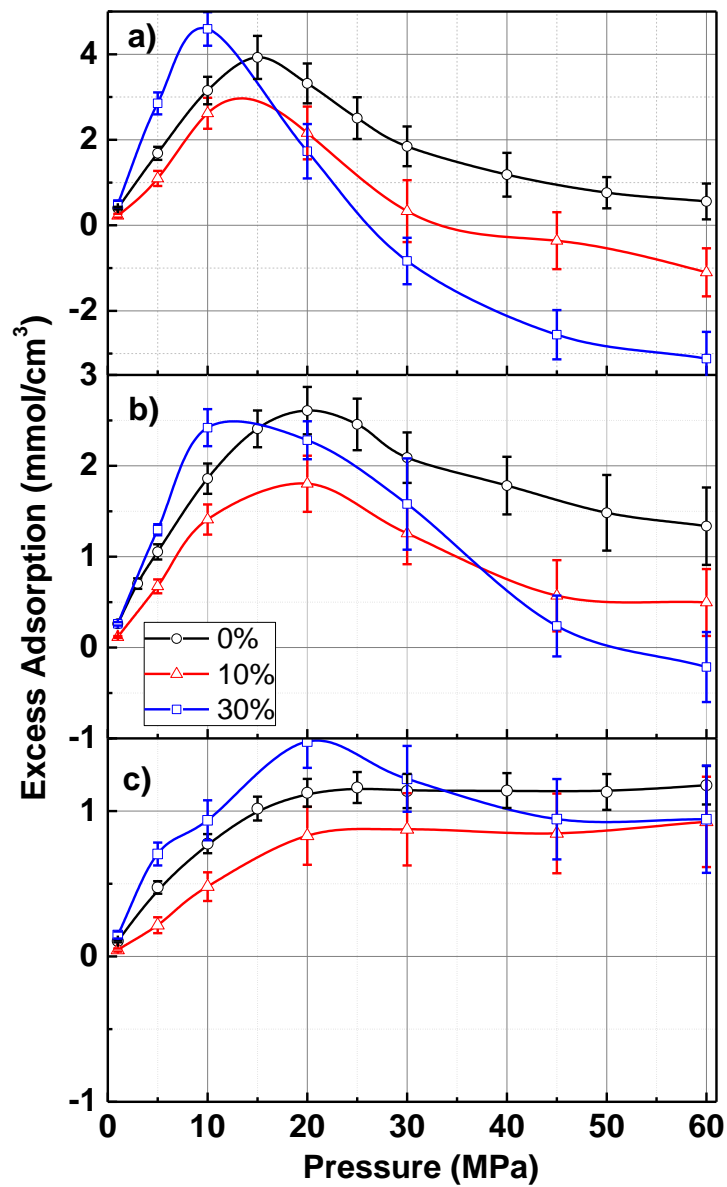


Fig. 3. Excess adsorption isotherms for a) CO<sub>2</sub> and b) CH<sub>4</sub> at RH 0% (black), 10% (blue), and 30% (red).



**Fig. 4.** CH<sub>4</sub> excess adsorption isotherms for a) 0.2:0.8, b) 0.5:0.5, and c) 0.8:0.2 CO<sub>2</sub>/CH<sub>4</sub> mixtures on illitic surface with tetrahedral substitutions and RH 0%, 10%, and 30%.



**Fig. 5.** CO<sub>2</sub> excess adsorption isotherms for a) 0.8:0.2, b) 0.5:0.5, and c) 0.2:0.8 CO<sub>2</sub>/CH<sub>4</sub> mixtures on illitic surface with tetrahedral substitutions and RH 0%, 10%, and 30%.

614

615

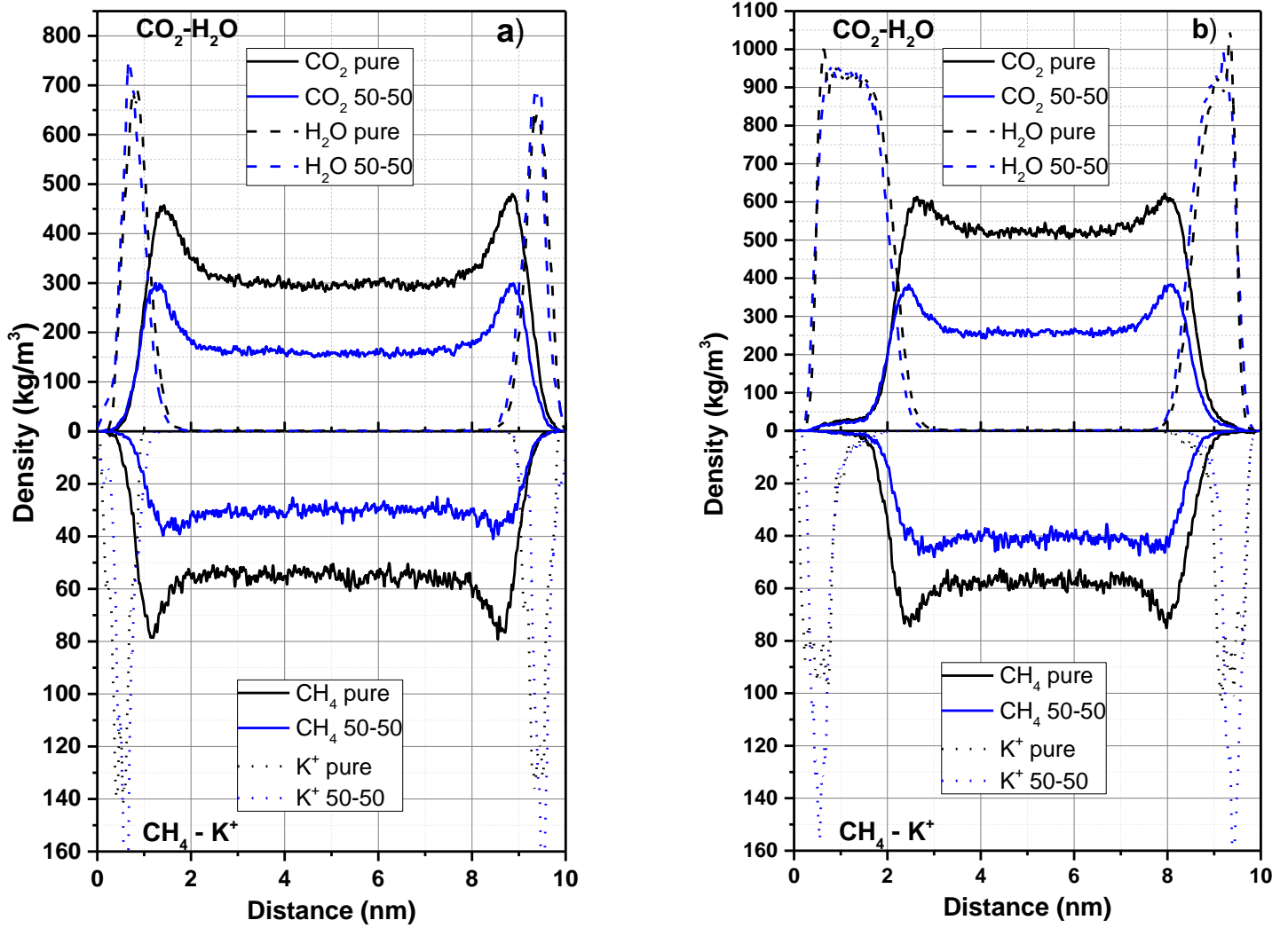
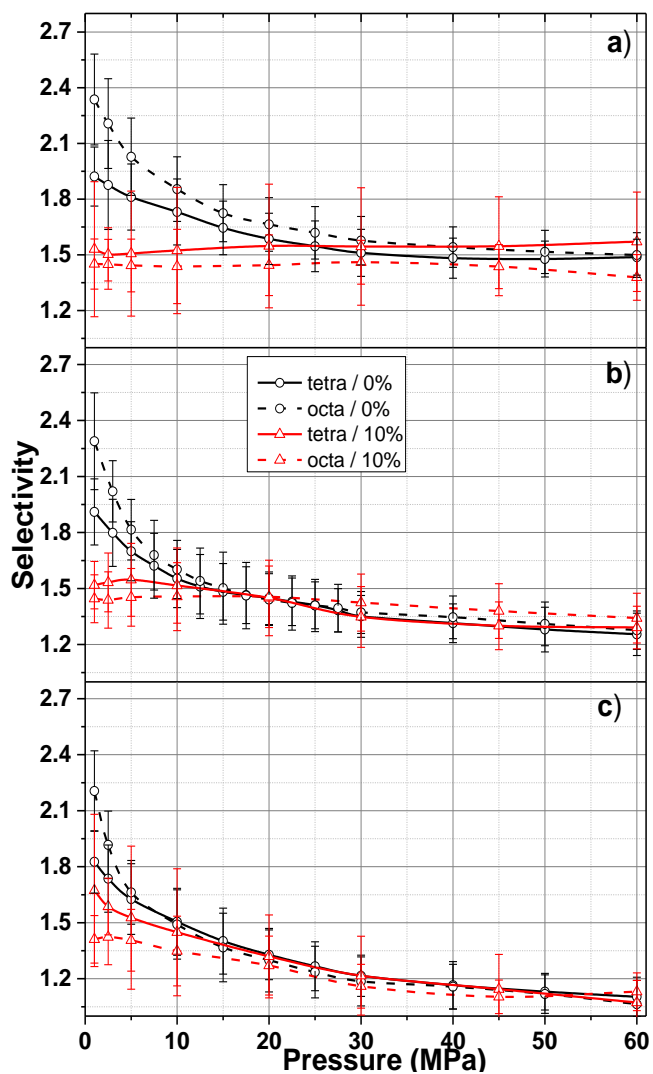


Fig. 6. Density distributions of carbon dioxide, methane, water, and potassium at 10 MPa and 355 K with RH a) 10% and b) 30% on illite surface with tetrahedral substitutions. 50-50 stands for 0.5:0.5 molar fractions of CO<sub>2</sub> to CH<sub>4</sub> in bulk mixtures.

616

617



**Fig. 7.** Selectivity parameters for adsorption of CO<sub>2</sub> and CH<sub>4</sub> on dry and wet illite surfaces at 355 K for **a)** 0.2:0.8, **b)** 0.5:0.5, **c)** 0.8:0.2 CO<sub>2</sub>/CH<sub>4</sub> compositions.

618

619

620

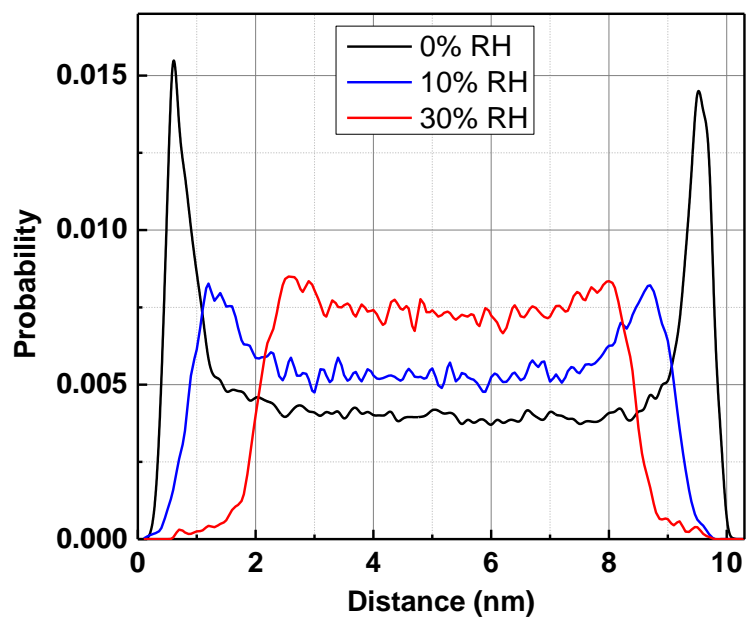


**Fig. 8.** Angle probability distribution for CO<sub>2</sub> molecules located near-parallel ( $0\pm 20$  degrees) to the clay surfaces in octahedral substituted illite at 10 MPa.

621

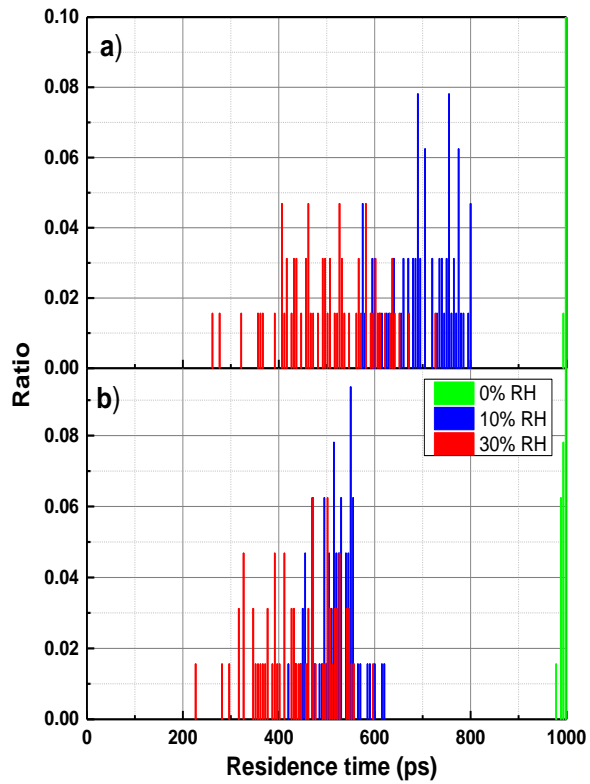


**Fig. 9.** K<sup>+</sup> ion residence times at **a)** octahedral and **b)** tetrahedral substituted illite surface with CO<sub>2</sub> and variable water content in pore space at 10 MPa.

622